ACS APPLIED MATERIALS & INTERFACES

Research Article

Cite This: ACS Appl. Mater. Interfaces 2019, 11, 14567−14575

www.acsami.org

Fully Stretchable Capillary Microfluidics-Integrated Nanoporous Gold Electrochemical Sensor for Wearable Continuous Glucose Monitoring

Chan Wool Bae,[†] Phan Tan Toi,[†] Bo Yeong Kim,[‡] Won Il Lee,[§] Han Byeol Lee,[†] Adeela Hanif,[†] Eung Hyuk Lee,[‡] and Nae-Eung Lee*[,†,‡,§]

[†]School of Advanced Materials Science & Engineering, [‡]SKKU Advanced Institute of Nano Technology (SAINT), and [§]Samsung Advanced Institute for Health Sciences & Technology (SAIHST), Sungkyunkwan University, 2066 Seobu-ro, Jangan-gu, Suwon, Gyeonggi-do 16419, Korea

Supporting Information

ABSTRACT: Biosensor systems for wearable continuous monitoring are desired to be developed into conformal patch platforms. However, developing such patches is very challenging owing to the difficulty of imparting materials and components with both high stretchability and high performance. Herein, we report a fully stretchable microfluidics-integrated glucose sensor patch comprised of an omnidirectionally stretchable nanoporous gold (NPG) electrochemical biosensor and a stretchable passive microfluidic device. A highly electrocatalytic NPG electrode was formed on a stress-absorbing 3D micropatterned polydimethylsiloxane (PDMS) substrate to confer mechanical stretchability, high sensitivity, and durability in non-enzymatic glucose detection. A thin, stretchable, and tough microfluidic device was made by embedding stretchable cotton fabric as a capillary into a thin polyurethane nanofiber-reinforced PDMS channel, enabling collection and passive, accurate delivery of sweat from skin to the electrode surface, with excellent replacement capability. The integrated glucose sensor patch demonstrated excellent ability to continuously and accurately monitor the sweat glucose level.

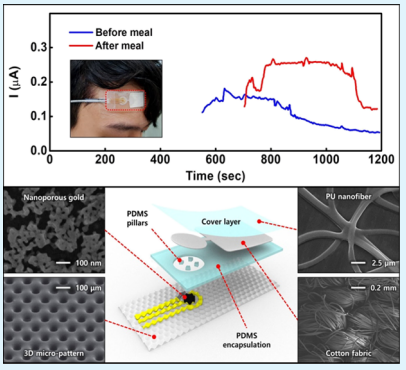

KEYWORDS: *stretchable electronics, non-enzymatic biosensor, nanoporous gold, stretchable microfluidic, continuous glucose monitoring*

1. INTRODUCTION

With the advent of smart healthcare, there has been a great deal of recent attention to the possibility of developing wearable biosensing systems that can monitor human physiological parameters, such as metabolites[1−16] and ions,[1−5,17−24] in body fluids, such as sweat,[1−9,11,12,16−18,20−26] interstitial fluid,[6,10] saliva,[13,15] and wound fluid,[14,19] in a continuous and noninvasive way, or diagnose diseases. In particular, wearable electrochemical biosensor patches for continuous monitoring of sweat glucose level have been considered as a promising approach for personal diabetes management; such a technology could obviate the need for inconvenient finger pricking to collect blood for portable enzymatic glucometers.[1−3] For user convenience in wearing an electrochemical biosensor patch, conformal contact with soft skin is preferred; this requires imparting mechanical stretchability to materials and components.[27] During the wearer's normal activities, alleviating motion-induced artifacts is essential to avoid sensing signal interference. Straining of materials and devices can complicate the sensor signal output and degrade the reliability of the patch. Recently, there have been reports on the use of stretchable tracks of Au nanosheets[28] or elastomeric composites,[29,30] or the use of an island-bridge approach using a flexible working electrode and serpentine tracks.[31] However, some limitations remain in imparting multidirectional stretchability to the sensor itself and ensuring electrical stability under repeated stretching cycles.[2]

Additional considerations are necessary in the realization of a stretchable electrochemical biosensor patch to fulfill the stability and accuracy requirements of monitoring operation. Wearable electrochemical biosensors based on enzymes are very sensitive to environmental conditions, such as temperature and pH, and cannot recover their characteristics after denaturation.[32,33] Such limitations prevent long-term storage ability or continuous monitoring functionality. Furthermore, for continuous monitoring of sweat glucose level with high accuracy over extended periods of time, there is a strong need for integrating microfluidic devices for continuous replenishment of sweat on the sensing electrode during measurement. Imparting mechanical stretchability to microfluidic devices and achieving minimal power consumption, thin form factor and

Received: January 14, 2019
Accepted: April 3, 2019
Published: April 3, 2019

DOI: 10.1021/acsami.9b00848
ACS Appl. Mater. Interfaces 2019, 11, 14567−14575

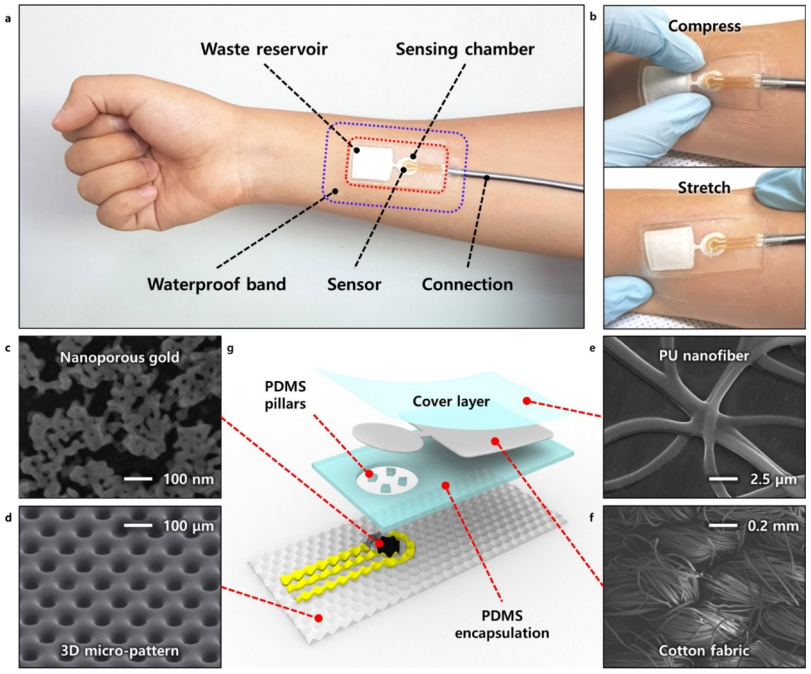

Figure 1. Schematic of stretchable microfluidics-integrated biosensor patch. (a) Photograph of fabricated patch mounted on the human body. (b) Photograph demonstrating conformality of the patch to human skin under compression or stretching. FE-SEM images of (c) NPG electrochemical electrode (top view), (d) 3D micropatterned PDMS substrate, (e) PU nanofiber, and (f) stretchable cotton fabric. (g) Layered components in the fully stretchable microfluidics-integrated biosensor patch.

durability are also of importance in designing for integration with stretchable biosensors in a wearable platform.

Thus, to realize daily sweat glucose monitoring using wearable electrochemical biosensors, many attributes, including detection accuracy, sensitivity, stability, user convenience, and cost-effectiveness, should be achieved, comparable to those of the electrochemical biosensor strips used in blood glucose meters. Wearable biosensor systems meeting all these attributes are still far from a reality. Herein we present a fully stretchable sweat glucose sensing patch integrated with a highly sensitive stretchable non-enzymatic nanoporous gold (NPG) biosensor and a stretchable, passive, and durable capillary microfluidic device. The NPG glucose sensor showed great sensitivity to glucose (253.4 μA cm^{-2} mM^{-1}), selectivity to interfering biomolecules, and mechanical durability, with no degradation after 1000 cycles of stretching to 30% strain. The fully stretchable integrated biosensor patch showed accurate sample handling capability for more accurate detection in wearable continuous glucose monitoring.

2. RESULTS AND DISCUSSION

2.1. Design of Stretchable Microfluidics-Integrated Biosensor Patch. The fabricated fully stretchable microfluidics-integrated biosensor patch attached on human body is shown in Figure 1a. The sensor patch is well adjusted to skin deformations of compression and stretching (Figure 1b). Stretchable NPG was used as the working electrode of the biosensor to allow sensitive non-enzymatic glucose sensing and high selectivity in the presence of interfering species (Figure 1c). To impart multidirectional stretchability to the normally very brittle NPG, an NPG working electrode together with an Au counter and Ag/AgCl reference electrodes was formed directly on a polydimethylsiloxane (PDMS) substrate in a mogul pattern comprising curvilinearly connected bumps and valleys for efficient stress absorption[34] (Figure 1d). In addition, we also developed a very thin, tough, and stretchable sample handling device based on very thin PDMS, reinforced by polyurethane nanofibers (PUNFs) (Figure 1e), and embedded with cotton fabric as a capillary material. This fabric is stretchable and has excellent capacity for liquid absorption and capillary flow even in highly stretched conditions (Figure 1f). We assembled the NPG electrochemical sensor and the PUNF-reinforced microfluidic device to form a fully stretchable microfluidics-integrated biosensor patch (Figure 1g).

2.2. Fundamental Properties of the NPG Electrode. NPG was formed by means of dealloying of vacuum-deposited Au:Ag alloys (~300 nm in thickness) on a substrate of SiO_2 wafer or 3D micropatterned PDMS (see details in Figure S1). Structural investigation of NPG indicated increased pore size of the nanoporous structure and decreased thickness with increasing dealloying time (Figure S2). Chemical examination showed that a trace amount of silver (~0.92 wt %) remained in the NPG even after 5 min of dealloying (Figure S3). Electrochemical characterization showed that increasing the dealloying time reduced the electrochemically active surface area of the NPG, consistent with the observation of increased pore size (Figure S4). Therefore, 5 min of dealloying is enough to form an NPG electrode with small pores (~30 nm) and high surface area.

2.3. Performance of Stretchable Non-Enzymatic Glucose Biosensor. A stretchable non-enzymatic glucose sensor was fabricated on a mogul-patterned PDMS substrate (Figure 2a) by means of direct formation of the gold patterns for tracks/electrodes and subsequent dealloying (5 min) to selectively form NPG and Ag/AgCl layers on the working and reference electrode surfaces, respectively. We confirmed that the NPG layer formed was uniform, with no significant cracking in either the bump or the valley areas of the mogul-

DOI: 10.1021/acsami.9b00848
ACS Appl. Mater. Interfaces 2019, 11, 14567−14575

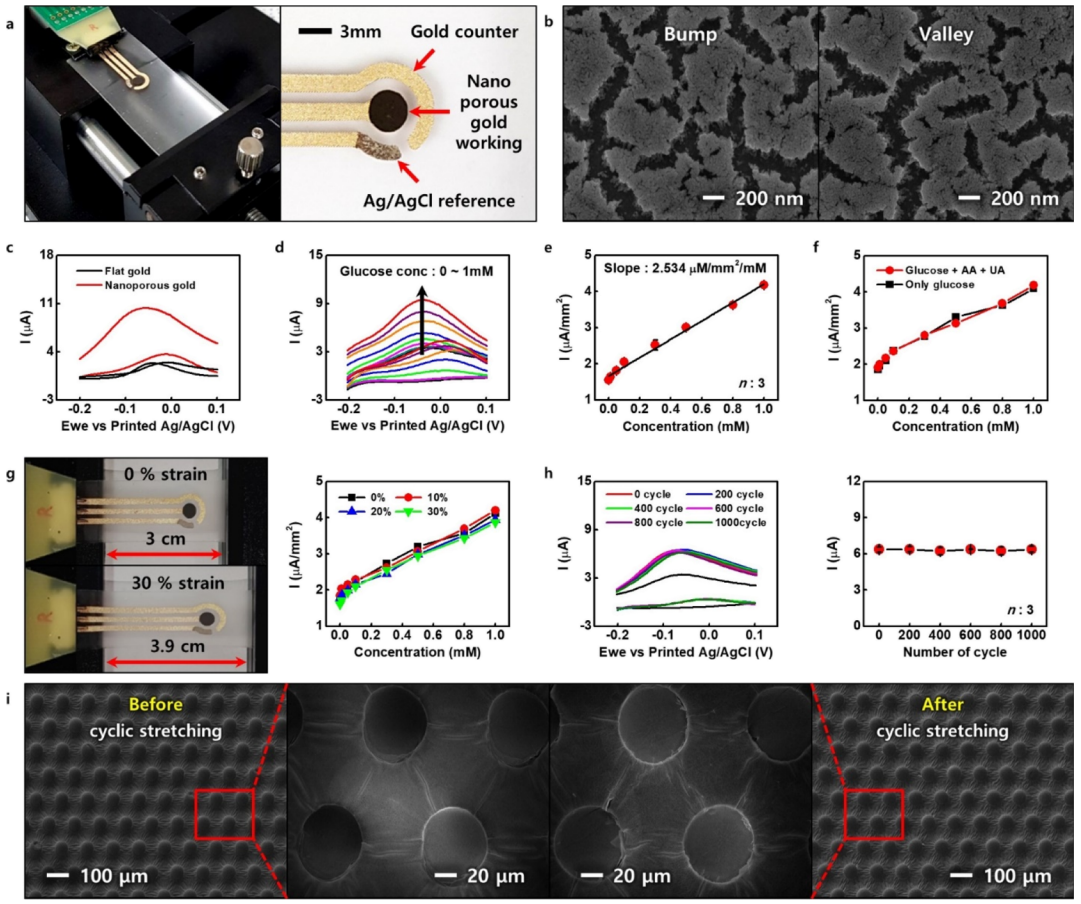

Figure 2. Fabrication and performance of stretchable non-enzymatic glucose sensor. (a) Optical images of fabricated sensor (with no microfluidic channel) and of the device loaded onto a jig for electrochemical characterization. (b) FE-SEM images of NPG structure in bump (left) and valley (right) of 3D micropatterned PDMS substrate. (c) CV responses of flat Au film (black) and NPG working electrode (red). The glucose sensing signal of the NPG working electrode was enhanced by a factor of 4.6 compared to that of a flat gold electrode. (d) CV responses and (e) calibration curve of the device under various glucose concentrations (0.01−1 mM). (f) CV responses of solutions of glucose only (0.01−1 mM) (black) and of glucose solutions (0.01−1 mM), including interferents (AA: 10 μM; UA: 10 μM) (red). (g) Optical image of the stretchable glucose sensor (left) and calibration curve with varying the elongation strain (0−30%) (right). (h) CV current response (left) and oxidation current signal (right) of the glucose sensor after various numbers of stretching cycles (glucose: 300 μM; black line: 0 μM). (i) FE-SEM images of NPG working electrode surfaces before (left) and after (right) cyclic stretching (1000 cycles at 30% strain).

patterned PDMS substrate (Figure 2b). The cyclic voltammetry (CV) response of the glucose sensor was measured using various scan rates under stretching of the sensor in various directions. The sensor showed good linearity of redox peak magnitude versus scan rate (10−100 mV/s) and less than 10% current change under multidirectional stretching (Figure. S5). CV measurements conducted to identify the non-enzymatic glucose oxidation of the fabricated glucose sensor showed two oxidation peaks near −0.2 and 0 V during the positive potential scan (Figure S6). The response current of the sensor was 4.6 times that of a flat gold electrode under equal conditions of glucose concentration and working electrode area (2.25 mm^2) (Figure 2c). CV measurements were conducted over the glucose concentration range of 0.01−1 mM (Figure 2d), which covers the sweat glucose concentration range of both hypoglycemic and hyperglycemic patients (0.02−0.6 mM);[35] these showed sensitivity as high as 253.4 $\mu A\ cm^{-2}\ mM^{-1}$ with good reproducibility (Figure 2e) and excellent selectivity in the presence of the strongly interfering biomolecules, ascorbic acid and uric acid (Figure 2f). Tuning of the surface roughness and surface area of the NPG electrode to enhance the glucose signal over the interferent signals can be utilized to solve the problem of selective detection of glucose in sweat. Glucose molecules with sluggish reaction rate compared to other interferent molecules can enter the rough surface more deeply and interact with the whole electrode surface, whereas the interferent molecules interact with the entrance area of the electrode and depleted from the outermost surface of electrode.[36]

To evaluate durability against mechanical deformations, we performed various stretching tests at different strain levels and with various numbers of stretching cycles. The CV response and the calibration curves of the glucose sensor under various applied strains of 0−30% (Figures S7 and 2g, respectively) indicated no significant change in either sensitivity or absolute current level throughout the entire strain range. Also, the CV responses and current changes of the glucose sensor were measured after the application of various numbers of stretching cycles; the response current was quite stable throughout continued cycling (Figure 2h). Moreover, after 1000 stretching cycles to 30% strain, only a few cracks were generated and no delamination of the NPG electrode was observed (Figure 2i). Dependence of glucose oxidation upon pH and temperature was also studied (Figure S8). The current signal changes

DOI: 10.1021/acsami.9b00848
ACS Appl. Mater. Interfaces 2019, 11, 14567−14575

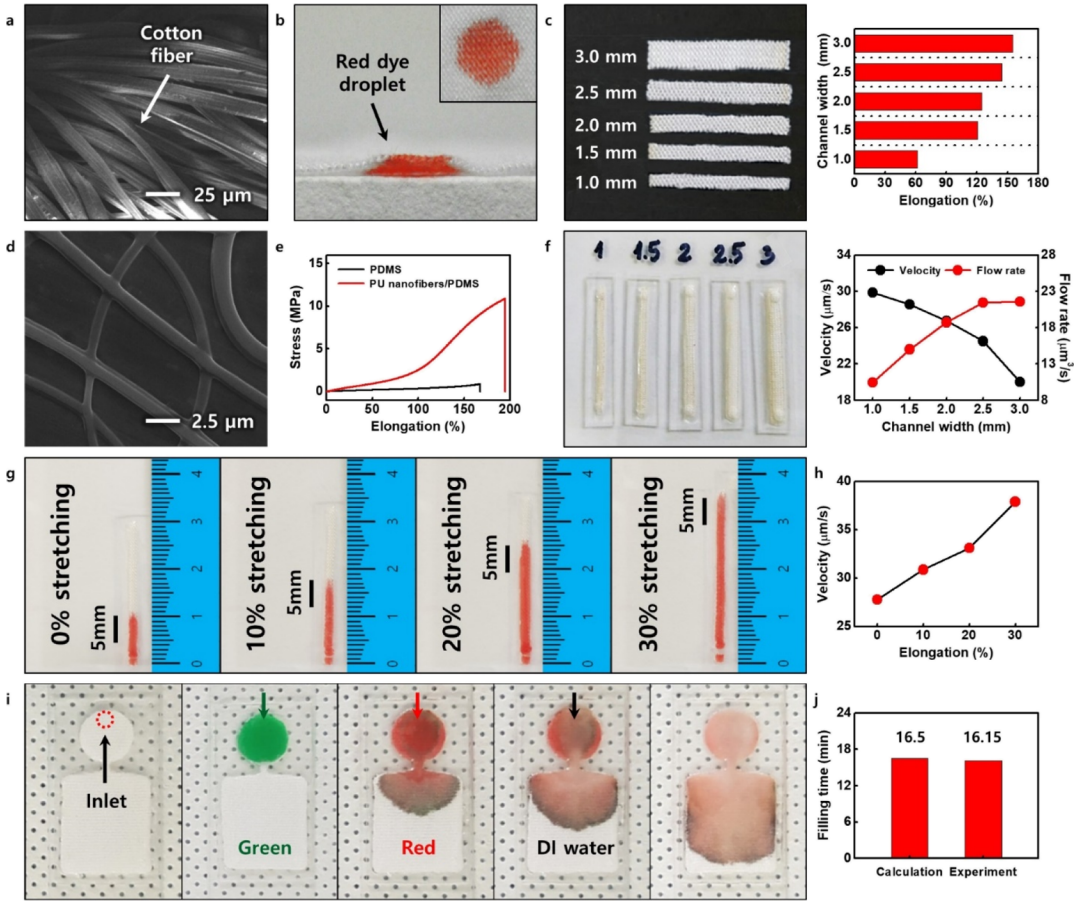

Figure 3. Fluid flow characteristics of fabricated thin microfluidic channel based on stretchable cotton fabric as a capillary. (a) FE-SEM image of cotton fabric. (b) Optical images of a 5 μL droplet of dyed deionized water on cotton fabric. (B, inset) Top-view optical image. (c) Optical images (left) and elongation at break (right) of cotton fabrics of various widths. (d) FE-SEM image of the surface of PUNF-reinforced PDMS. (e) Stress–strain curve of PUNF-reinforced PDMS used as a bottom substrate layer for fabrication of thin microfluidic channels. (f) Optical images (left) and volumetric flow rate and fluid velocity (right) of straight microfluidic channels of various widths. For each straight channel, the inlet was supplied with red dyed DI water at a rate of 0.05 mL/h by a syringe pump. In each test, the time elapsed was measured until the dye reached the distance of 1 cm from the inlet. (g) Optical images and (h) fluid velocities of straight microfluidic channel (1.5 mm width) under various applied strains (0–30%). A syringe pump was used to supply dyed DI water to the inlet at a rate of 0.05 mL/h. The flow pattern was observed at every 5 mm interval of flow distance under each stretching condition. (i) Optical images of the fabricated sample handling device during sequential replacement by different dyed solutions and undyed water. The injection rate of each fluid used was 1.67 μL/min. (j) Measured and calculated filling times of the sensing chamber (circular shape) in the sample handling device.

induced by static elongation, cyclic stretching, pH change, and temperature change were recalculated as concentration change ratios, and the relative errors that can be induced by these four parameters were compared (Figure S9). The results showed that the sensor signal depended only upon the pH of the glucose solution.

2.4. Liquid-Driving Characteristics of Stretchable Microfluidic Channel. As a stretchable capillary material, a stretchable cotton fabric was used having a plain knit structure, including bundles of cotton fibers 10 μm in diameter (Figure 3a). It could be seen that the fabric was hydrophilic (Figure 3b). Stretchability of cotton fabric strips of various widths (1–3 mm) was investigated; the breaking points of the strips except the 1 mm wide strip were over 120% their original widths (Figure 3c). Bundles of fibers in strips under mechanical stretching (0–60%) were pulled out and formed gaps between the bundles, which became larger with increasing elongation. Furthermore, the fabric structure was clearly maintained under repeated deformation of 1000 stretching cycles to 50% strain and recovered to its original structure after release. For fabrication of a capillary microfluidic channel, the stretchable cotton fabric was integrated into an elastomeric PUNF-reinforced PDMS substrate. Because of the requirement of a very thin microfluidic device for high conformality, the bottom PDMS layer of the microfluidic device was reinforced by embedding it with highly compliant PUNFs; the resulting material maintained the stretchability of PDMS despite this reinforcement (Figure 3d). The strain–stress curve of the resulting PUNF-reinforced PDMS (~90 μm) showed a higher Young's modulus (increased by a factor of up to about 13 at high strain level) compared to that of a layer of unmodified PDMS of the same thickness (Figure 3e). The PUNF-reinforced PDMS had a strain-induced stiffening effect because of the stiffer embedded PUNFs, resulting in a skin-like self-limiting mechanical property.[37,38] The excellent mechanical properties of the nanocomposite PDMS allowed us to fabricate soft microfluidic channels to be much thinner and more stretchable but also tougher, which could improve their conformal attachment to skin and allow more facile integration with a sensor layer compared to a thick layer of bare PDMS.

DOI: 10.1021/acsami.9b00848
ACS Appl. Mater. Interfaces 2019, 11, 14567–14575

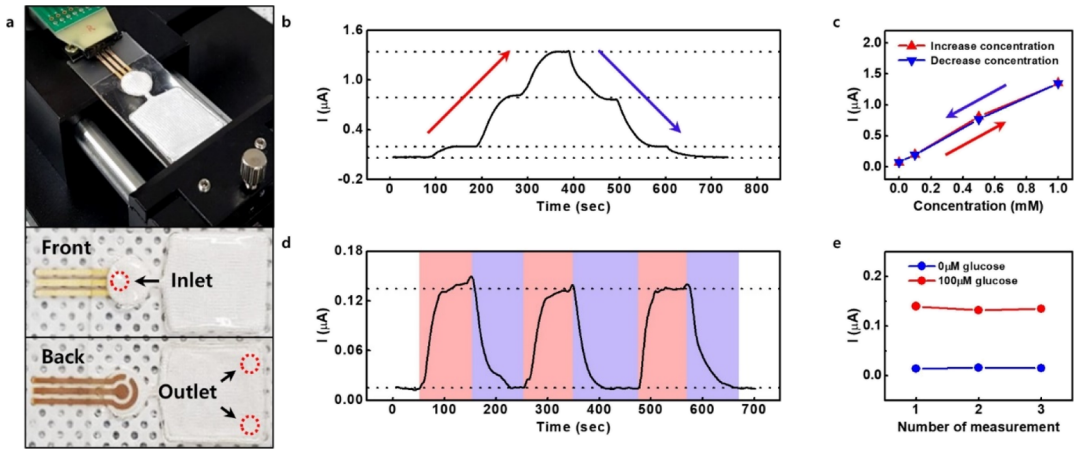

Figure 4. Performance of stretchable microfluidics-integrated biosensor patch. (a) Optical images of the patch loaded onto a jig for measurement (top) and of the patch showing its front and backside (bottom). There was one inlet to absorb sample solution at the front side of the patch and two outlets to drain air at the back side. (b) Real-time CA response of the biosensor patch during changes in glucose concentration in artificial sweat: stepped increases from 0 to 1 mM and stepped decreases from 1 to 0 mM. (c) CA response current values obtained from the real-time CA response data in part (b) under the increasing and decreasing steps of glucose concentration. (d) Real-time CA response of the biosensor patch in response to repeated alternating injections of artificial sweat solutions of glucose concentrations 100 and 0 μM. (e) Current signal of the biosensor patch during the repeated injections. Each measurement was performed with 120 μL of artificial sweat solution, with a waiting period of about 100 s to allow complete absorption.

Liquid flow characteristics of cotton fabric were investigated of fabricated straight microfluidic channels of widths 1−3 mm, each having one hole at each end of the channel as an inlet and an outlet (left, Figure 3f). With increasing channel width, the fluid velocity gradually decreased and the flow rate increased (right, Figure 3f). These results were modeled well by the Young−Laplace equation, which describes capillary action as a function of the cross-sectional dimension of a capillary channel.[39−42] The liquid transport behavior was studied in the stretchable microfluidic material having a channel 1.5 mm in width under various stretching conditions of 0−30% (Figure 3g). The measured velocity of the flow increased linearly with increasing elongation (Figure 3h). Table S1 lists the calculated velocities. These results can be easily explained in terms of the narrowing of the channel under stretching, in a manner consistent with the observation of increasing velocity with decreasing channel width (Figure 3g).

2.5. Characterization of Stretchable Fabric-Based Sample Handling Device. On the basis of the characterization results of stretchable straight microfluidic channels, we designed and fabricated a sample handling device for sweat collecting and transporting purposes. For our sample handling device, the filling time, which is the duration of flow required to fill the whole area of the sensing chamber with green dyed deionized (DI) water, was measured to be 16.15 min (Figure 3i) and theoretically calculated to be 16.5 min based on the dimensions of the design (Figure 3j and Table S2). To confirm the continuous replenishment of the sensing chamber by fresh incoming fluid, dyed and pure DI water were sequentially injected (Figure 3i). Following the initial filling of the sensing chamber by green dyed water, red dyed water was immediately used to fill the device, showing the same filling time used for the green dyed water. Finally, flushing the device with pure DI water washed out the red dyed water almost completely.

2.6. Performance of Stretchable Microfluidics-Integrated Biosensor Patch. The fabricated stretchable microfluidics-integrated biosensor patch and its specific scales are shown in Figures 4a and S10, respectively. To evaluate the wetting property of the electrodes in the biosensor patch, we attached a PDMS well directly on the sensing chamber and simply applied droplets of artificial sweat. Monitoring of the open circuit potential gave the time at which the sensing chamber was fully wetted (Figure S11). When wetting is not sufficient, the sensor will generate a false signal; this represents a serious hurdle to continuous monitoring.[2] For this reason, identification of wetting and maintenance of the solution volume in the sensing chamber even during sample replacement are critically important for continuous monitoring. Therefore, we set the size and number of inlets by considering the absorption rate of the fabric and the channel width to maintain a constant solution volume in the chamber.

To evaluate the continuous glucose-sensing ability of the biosensor patch, we carried out chronoamperometric (CA) measurements (Figure 4b). After wetting of the sensing chamber, artificial sweat samples containing 100, 500, and 1000 μM glucose were sequentially added; the signal increased immediately but slowly, and then became saturated. We also applied the artificial sweat samples in the order of decreasing concentration, observing a decrease in the current signal with decreasing glucose concentration. The linearity of the CA signal of the patch showed almost the same sensitivities during the application of increasing (57.56 μA cm^{-2} mM^{-1}) or decreasing glucose concentrations (57.24 μA cm^{-2} mM^{-1}) (Figure 4c). However, a glucose sensor without the sample handling device showed different CA responses (Figure S12). When increasing the glucose concentration, because of a dilution effect by residual solution with lower glucose concentration (Table S3), the current level was much lower than expected. In contrast, when decreasing the glucose concentration, the current level was much higher than expected (Table S3) because of an enrichment effect by residual solution with higher glucose concentration. Comparison of the CA response currents clearly showed a concentration hysteresis in the case of incomplete replacement of the solutions because of solution mixing in the case of the biosensor having a PDMS well, but no such hysteresis in the

DOI: 10.1021/acsami.9b00848
ACS Appl. Mater. Interfaces 2019, 11, 14567−14575

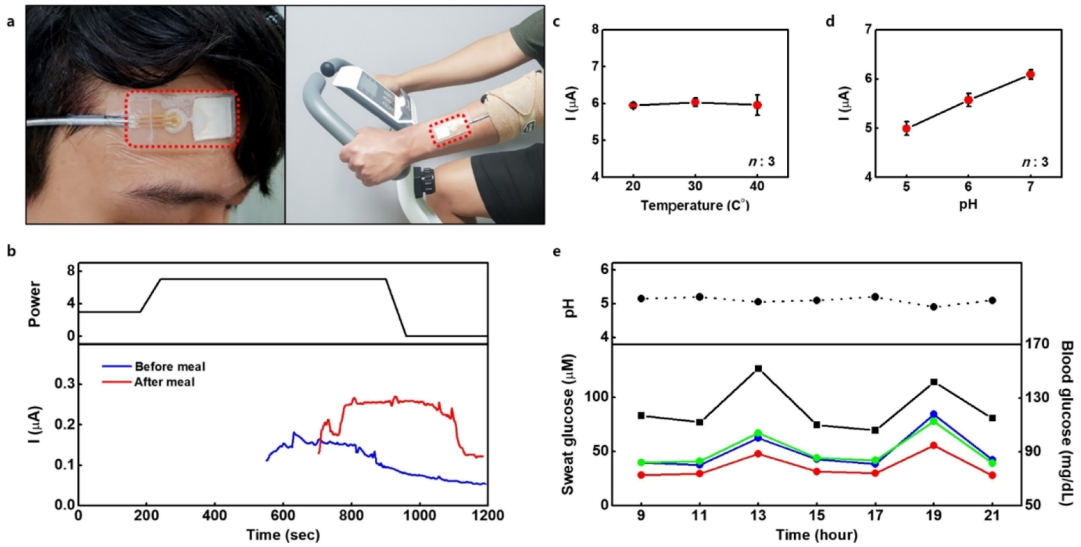

Figure 5. Continuous measurement of sweat glucose levels and accuracy testing. (a) Optical images of the stretchable microfluidics-integrated biosensor patch attached on the forehead (left) or arm (right) of a subject. (b) Real-time measurement of the biosensor patch attached to the forehead. (c,d) Changes in sensing signal under various conditions of (c) temperature (20, 30 and 40 °C) and (d) pH (5, 6 and 7). (e) One-day monitoring results of pH level (top) and glucose level (bottom) in sweat measured by the patch, before pH compensation (red) and after pH compensation (green), a commercial sweat assay kit (blue), and glucose level in blood (black). The subject had meals at 12 and 6 PM on this day, and the blood was collected just before the subject rode the cycling machine, considering the time delay (~20 min) in blood and sweat glucose concentration.

case of the biosensor patch integrated with a microfluidic sample handling device (Figure S13).

We next evaluated the fouling effect expected to be caused by absorption of glucose reaction byproducts during repetitive measurement (Figure 4d). The biosensor patch showed consistent responses during repeated replacement of artificial sweat having low glucose concentration, indicating that the byproducts were completely pushed into the reservoir from the chamber by incoming solution (Figure 4e).

2.7. Continuous Measurement of Sweat Glucose Level and Accuracy Testing. Then, we connected our biosensor patch with a portable potentiostat and attached it onto the forehead or arm of a subject while they rode a cycling machine for 20 min to produce sweat for sampling and measurements (Figures S14 and 5a). After about 10 min of cycling, the sensing chamber was completely wetted by real sweat, and the CA current level increased and was saturated stably for a while. There was a clear difference in the signals of tests conducted before and after meals; in both cases, the CA signal dropped sharply after the subject stopping cycling (Figure 5b). This phenomenon arose from the problem of keeping wet the electrode surfaces in the sensing chamber. After the subject stopped cycling, their sweating slowed. However, in the meantime, the sweat in the sensing chamber flowed out into the reservoir, leading to poor wetting of the electrode surfaces and a sharp drop in the signal.

Next, sweat glucose level monitoring for one day was performed after 20 min of cycling, using the stretchable microfluidics-integrated biosensor patch. For comparison, the glucose levels in the blood and sweat were also measured by using a commercial glucose meter and glucose assay kit, respectively. Changes in the sensing signal of the patch under variations in measurement temperature (Figure 5c) and pH (Figure 5d) indicated that the concentration reading was affected by sweat pH only. Therefore, to allow calibration, the pH level in the collected sweat was also measured with a commercial pH sensor. All results of the sweat glucose monitoring are summarized in Figure 5e. Similar to other studies,[7] sweat pH level did not change significantly before and after meals or exercise, but glucose concentration did change significantly before and after meals. The pH calibration made the glucose-sensing results of our biosensor patch more closely match the commercial sweat glucose assay in terms of both the tendency and the absolute value of concentration. The accuracy test results of the biosensor patch are compared with those of the glucose assay in Figure S15.

3. CONCLUSIONS

NPG is suitable for a broad range of applications, including biosensors, because of its high electrochemical catalytic effects, high surface area, great chemical stability, and various available manufacturing methods.[43,44] However, NPG undergoes brittle fracture in tensile deformation despite the ductility of bulk gold, although the mechanical properties change depending on the manufacturing method and the diameter of the ligament.[45,46] In this work, structural engineering of brittle NPG by using a 3D micropatterned elastomeric substrate that can effectively absorb the stress generated during stretching enabled the realization of a stretchable non-enzymatic electrochemical glucose biosensor. For the concept of a wearable glucose-sensing platform integrated with stretchable NPG electrochemical sensor, a very thin microfluidic channel for better conformal attachment to the human body could be realized using a stretchable cotton fabric and a PUNF-reinforced PDMS layer with reduced thickness, but high toughness and good stretchability. Finally, we integrated two parts in a simple way and confirmed that the sweat sample could be effectively collected, flowed smoothly through the stretchable cotton fabric channel from the sensing chamber to the reservoir, and could be replaced well even during repeated exchange, thereby allowing accurate measurement of sweat glucose level. In conclusion, a fully stretchable microfluidics-

DOI: 10.1021/acsami.9b00848
ACS Appl. Mater. Interfaces 2019, 11, 14567−14575

integrated biosensor patch with high sensitivity, stretchability, durability, and accuracy in continuous on-body sensing shows great potential for continuous monitoring of metabolites, including glucose, not only in sweat but also in other body fluids.

4. METHODS

4.1. Fabrication of Stretchable Non-Enzymatic Glucose Biosensor. The stretchable non-enzymatic glucose sensor was fabricated as follows (Figure S16a–c). Thin Al_2O_3 (3 nm) was first deposited by means of atomic layer deposition, an adhesion layer of Ti (10 nm) was deposited by means of e-beam deposition, and tracks of Au (50 nm) were deposited by means of thermal evaporation, directly onto a 3D mogul-patterned PDMS (Sylgard 184, Dow Corning) substrate for working, counter, and reference electrodes. Then, Au and Ag were deposited simultaneously for 20 min with the deposition rate ratio of 1:9 to make an Au–Ag alloy on the sensing area of the working electrode only, using a stencil mask. The deposited electrodes were dipped in nitric acid (7697-37-2, Samchun) for 5 min to dealloy them and then were rinsed with DI water. Then, to form a Ag/AgCl reference electrode, 1.5 g of Ag/AgCl ink (011464, BAS Inc.) was mixed with 1.5 g of ethyl acetate (141-78-6, Sigma-Aldrich) and 100 μL of Zonyl FS-300 (197664-69-0, Sigma-Aldrich) was added to improve bonding strength. After completely mixing these three components, 10 wt % Ecoflex (EcoFlex 00-30, Smooth-on Inc.) was added to impart mechanical compliance, and the resulting mixture was allowed to stand for 6 h to allow full dispersion. The prepared paste was printed on the region of the reference electrode only by using a stencil mask and was cured at 120 °C for 10 min.

4.2. Characterization of Stretchable Non-Enzymatic Glucose Biosensor. To investigate the electrochemical characteristics of fabricated stretchable non-enzymatic glucose sensors with various design variables, CV measurements were performed using a potentiostat (VSP, Bio-Logic). All measurements were performed in phosphate buffer (pH 7.5, Sigma-Aldrich), and electrochemical cleaning with 0.1 M sodium hydroxide (1310-73-2, Sigma-Aldrich) solution was carried out between each characterization measurement.

4.2.1. Characterization of NPG Electrode. Characteristics of the electrochemically active surface area of NPG electrodes subjected to various durations of dealloying were evaluated using 10 mM potassium ferricyanide (13746-66-2, Sigma-Aldrich) solution. The scan rate was fixed at 50 mV/s.

4.2.2. Sensitivity and Selectivity Test. We calibrated our glucose sensor using glucose (50-99-7, Sigma-Aldrich) solutions ranging between 0.01 and 1 mM concentration at a scan rate of 20 mV/s. Selectivity tests were performed using 10 μM ascorbic acid (AA) (50-81-7, Sigma-Aldrich) and 10 μM uric acid (UA) (69-93-2, Sigma-Aldrich), with the same glucose concentration range and scan rate used in the sensitivity tests.

4.2.3. Stretching Test. Stretching tests were performed with various applied strains (0, 10, 20, and 30%) and numbers of stretching cycles (0, 200, 400, 600, 800, and 1000 cycles at 30% elongation) in a custom-built cyclic stretching tester. The same glucose concentration range and scan rate were used as in the sensitivity tests.

4.2.4. pH and Temperature Dependence. The pH and temperature dependencies were evaluated with 300 μM glucose solution at various pH levels (pH 5, 6, and 7) and temperatures (20, 30, and 40 °C). The scan rate was fixed at 20 mV/s.

4.3. Fabrication of Stretchable Fabric-Based Microfluidic Channel. Stretchable cotton fabric was purchased at a local fabric market (Seoul, Republic of Korea). The fabric was cut into the designed channel pattern by using a laser cutter, ultrasonically washed in sodium hydroxide (1310-73-2, Sigma-Aldrich) solution for 15 min, rinsed with DI water, and dried at 60 °C under airflow for 2 h.

The stretchable fabric-based microfluidic channel was fabricated as follows (Figure S17). A 15 wt % polyurethane (SG-85A, Teco Flex) solution in *N*,*N*-dimethylformamide (68-12-2, Sigma-Aldrich) was prepared by stirring at 80 °C for 3 h. This PU solution was used to produce PUNFs by using a custom-built electrospinning machine. A syringe containing 0.2 mL PU solution was pumped at a speed of 1 mL/h. Between the collector of 10 cm × 10 cm area, consisting of five glass slides, and the 21-gauge nozzle, which was placed 15 cm from the collector, was applied a voltage of 15 kV to directly spin the PUNFs. Afterward, PDMS (Sylgard 184, Dow Corning) was poured on the glass slides containing the PUNFs. Bubbles in the nanofiber-embedded PDMS samples were removed by placing them in a vacuum desiccator, and the PUNF-embedded PDMS samples were further coated in a spin coater at 1000 rpm in 40 s to obtain substrates of thickness 90 μm after curing at 80 °C for 1 h.

Then, a designed stencil mask, which was cut by a laser cutter, was applied over PUNFs-reinforced PDMS substrate to make a channel pattern. Uncured PDMS (Sylgard 184, Dow Corning) was poured onto the substrate and spin coated at 800 rpm for 40 s. Subsequently, it was half-cured at 80 °C for 3 min to ensure high viscosity of the PDMS layer and thus to avoid its penetration under the mask. The stencil mask was peeled off immediately after the half-curing step, and the substrate was continued to be cured for 3 min at 80 °C to make the PDMS surface sticky. The patterned cotton fabric was then aligned into the preformed channel pattern, and another PUNFs-reinforced PDMS cover was attached. Finally, the fabricated microfluidic channel was completely cured by treatment in a hot-press machine at 80 °C for 1 h. To form inlet and outlet, the fabricated microfluidic channel was manually punched by using a 13-gauge needle.

4.4. Integration Process of Stretchable Microfluidics-Integrated Biosensor Patch. The stretchable microfluidics-integrated biosensor patch was fabricated using the following procedure (Figure S16d–f). To prevent contact between the cotton fabric and the sensor electrodes, four PDMS (Sylgard 184, Dow Corning) pillars were formed between the working and counter electrodes. After surrounding the sensing region of the electrodes with a Teflon tape barrier (ASK018AD, ALPHAFLON) to prevent PDMS penetration, a PDMS (Sylgard 184, Dow Corning) encapsulation layer was spin coated onto the sensor layer at 500 rpm for 10 s and cured at 80 °C for 2 min. It was further cured for 3 min after peeling off the Teflon tape barrier to make the PDMS surface stickier. Then, the patterned cotton fabric was aligned to the sensor region, and the thin PUNFs-reinforced PDMS cover for preventing unintentional wetting of the waste reservoir by extracted sweat was attached to the fabricated biosensor patch. Finally, the biosensor patch was cured at 80 °C for 1 h.

4.5. Characterization and On-Body Detection Demonstration of Stretchable Microfluidics-Integrated Biosensor Patch. To identify the electrochemical characteristics of the fabricated stretchable microfluidics-integrated biosensor patch, a desktop potentiostat (VSP, Bio-Logic) and a portable electrochemical analyzer (EmStat Blue 3+, Palm Instrument B.V.) were used.

4.5.1. Wetting Test. Open-circuit potential of the biosensor patch was measured for 60 s to evaluate the absorption rate of an artificial sweat solution of phosphate buffer (pH 7.5, Sigma-Aldrich) with 10 mM sodium chloride (7647-14-5, Sigma-Aldrich).

4.5.2. Solution Replacement Test. Chronoamperometry was performed with 120 μL artificial sweat in each step of increasing or decreasing concentration. The waiting time for complete absorption in each step was 100 s.

4.5.3. On-Body Detection and Accuracy Test. Copper wire leads were attached to each electrode of our sensor patch with silver paste (ELCOAT, CANS) to connect them to a portable electrochemical analyzer (EmStat Blue 3+, Palm Instrument B.V.). The portable electrochemical analyzer is controlled wirelessly using a PStouch Android application. The sensor patch was attached on the forehead or arm of our subject by means of a waterproof band (A-Derm, EVERAID) to prevent delamination and evaporation of sweat, and the subject (age: 25, male) rode a cycling machine for 20 min to produce sweat. Because the amount of extracted sweat was too less, we removed only the cover layer on the sensing chamber part to maximize sweat collection efficiency during the on-body detection. We compared the results of the sensor patch with the results of a

DOI: 10.1021/acsami.9b00848
ACS Appl. Mater. Interfaces 2019, 11, 14567–14575

glucose assay (Colorimetric glucose assay kit, Cayman Chemical) and glucose meter (CareSens N, I-sens). To allow pH correction of measured glucose concentration, the pH of the sweat was measured by using a pH sensor (Orion 3 Star, Thermo Scientific).

■ ASSOCIATED CONTENT

Supporting Information

The Supporting Information is available free of charge on the ACS Publications website at DOI: 10.1021/acsami.9b00848.

Fabrication process of NPG electrode (Figure S1); SEM images of NPG electrode (Figure S2); EDS spectrum of NPG (Figure S3); CV response of NPG electrode by various durations of dealloying (Figure S4); CV response of NPG electrode under various scan rate and stretching directions (Figure S5); glucose oxidation characteristics (Figure S6); mechanical deformation test (Figure S7); pH and temperature dependence test (Figure S8); current and re-calculated concentration change ratio under various conditions (Figure S9); design of sensor patch (Figure S10); wetting property of sensor patch (Figure S11); CA response of sensor patch without sample handling device (Figure S12); concentration hysteresis characteristic (Figure S13); on-body measurement system (Figure S14); accuracy test (Figure S15); fabrication process of biosensor patch (Figure S16); fabrication process of fabric-based microfluidic channel (Figure S17); flow velocity calculation (Table S1); calculation of liquid filling time (Table S2); reactant mixing effect (Table S3) (PDF)

■ AUTHOR INFORMATION

Corresponding Author

*E-mail: nelee@skku.edu.

ORCID

Nae-Eung Lee: 0000-0002-6539-5010

Author Contributions

C.W.B. and P.T.T. contributed equally to this work. C.W.B., P.T.T., B.Y.K., H.B.L., A.H., and N.E.L. designed the methodology. C.W.B., P.T.T., W.I.L., and E.H.L. performed the experiments. N.E.L. supervised the project. C.W.B., P.T.T., and N.E.L. wrote the paper. All authors discussed the results and contributed to the paper.

Notes

The authors declare no competing financial interest.

■ ACKNOWLEDGMENTS

This research was supported by the Basic Science Research Program (2016R1A2A1A05005423) of the National Research Foundation (NRF), funded by the Ministry of Science, ICT & Future Planning.

■ REFERENCES

(1) Gao, W.; Emaminejad, S.; Nyein, H. Y. Y.; Challa, S.; Chen, K.; Peck, A.; Fahad, H. M.; Ota, H.; Shiraki, H.; Kiriya, D.; Lien, D.-H.; Brooks, G. A.; Davis, R. W.; Javey, A. Fully Integrated Wearable Sensor Arrays for Multiplexed In Situ Perspiration Analysis. *Nature* **2016**, *529*, 509−514.

(2) Lee, H.; Choi, T. K.; Lee, Y. B.; Cho, H. R.; Ghaffari, R.; Wang, L.; Choi, H. J.; Chung, T. D.; Lu, N.; Hyeon, T.; Choi, S. H.; Kim, D.-H. A Graphene-Based Electrochemical Device with Thermoresponsive Microneedles for Diabetes Monitoring and Therapy. *Nat. Nanotechnol.* **2016**, *11*, 566−572.

(3) Lee, H.; Song, C.; Hong, Y. S.; Kim, M. S.; Cho, H. R.; Kang, T.; Shin, K.; Choi, S. H.; Hyeon, T.; Kim, D.-H. Wearable/Disposable Sweat-Based Glucose Monitoring Device with Multistage Transdermal Drug Delivery Module. *Sci. Adv.* **2017**, *3*, No. e1601314.

(4) Koh, A.; Kang, D.; Xue, Y.; Lee, S.; Pielak, R. M.; Kim, J.; Hwang, T.; Min, S.; Banks, A.; Bastien, P.; Manco, M. C.; Wang, L.; Ammann, K. R.; Jang, K.-I.; Won, P.; Han, S.; Ghaffari, R.; Paik, U.; Slepian, M. J.; Balooch, G.; Huang, Y.; Rogers, J. A. A Soft, Wearable Microfluidic Device for The Capture, Storage, and Colorimetric Sensing of Sweat. *Sci. Transl. Med.* **2016**, *8*, 366ra165.

(5) Choi, J.; Kang, D.; Han, S.; Kim, S. B.; Rogers, J. A. Thin, Soft, Skin-Mounted Microfluidic Networks with Capillary Bursting Valves for Chrono-Sampling of Sweat. *Adv. Healthcare Mater.* **2017**, *6*, 1601355.

(6) Kim, J.; Sempionatto, J. R.; Imani, S.; Hartel, M. C.; Barfidokht, A.; Tang, G.; Campbell, A. S.; Mercier, P. P.; Wang, J. Simultaneous Monitoring of Sweat and Interstitial Fluid Using a Single Wearable Biosensor Platform. *Adv. Sci.* **2018**, *5*, 1800880.

(7) Oh, S. Y.; Hong, S. Y.; Jeong, Y. R.; Yun, J.; Park, H.; Jin, S. W.; Lee, G.; Oh, J. H.; Lee, H.; Lee, S.-S.; Ha, J. S. Skin-Attachable, Stretchable Electrochemical Sweat Sensor for Glucose and pH Detection. *ACS Appl. Mater. Interfaces* **2018**, *10*, 13729−13740.

(8) Abellán-Llobregat, A.; Jeerapan, I.; Bandodkar, A.; Vidal, L.; Canals, A.; Wang, J.; Morallón, E. A Stretchable and Screen-Printed Electrochemical Sensor for Glucose Determination in Human Perspiration. *Biosens. Bioelectron.* **2017**, *91*, 885−891.

(9) Bandodkar, A. J.; Jia, W.; Yardımcı, C.; Wang, X.; Ramirez, J.; Wang, J. Tattoo-Based Noninvasive Glucose Monitoring: A Proof-of-Concept Study. *Anal. Chem.* **2015**, *87*, 394−398.

(10) Chen, Y.; Lu, S.; Zhang, S.; Li, Y.; Qu, Z.; Chen, Y.; Lu, B.; Wang, X.; Feng, X. Skin-Like Biosensor System via Electrochemical Channels for Noninvasive Blood Glucose Monitoring. *Sci. Adv.* **2017**, *3*, No. e1701629.

(11) Imani, S.; Bandodkar, A. J.; Mohan, A. M. V.; Kumar, R.; Yu, S. F.; Wang, J.; Mercier, P. P. A Wearable Chemical-Electrophysiological Hybrid Biosensing System for Real-Time Health and Fitness Monitoring. *Nat. Commun.* **2016**, *7*, 11650.

(12) Jia, W.; Bandodkar, A. J.; Valdés-Ramírez, G.; Windmiller, J. R.; Yang, Z.; Ramírez, J.; Chan, G.; Wang, J. Electrochemical Tattoo Biosensors for Real-Time Noninvasive Lactate Monitoring in Human Perspiration. *Anal. Chem.* **2013**, *85*, 6553−6560.

(13) Kim, J.; Valdés-Ramírez, G.; Bandodkar, A. J.; Jia, W.; Martinez, A. G.; Ramírez, J.; Mercier, P.; Wang, J. Non-Invasive Mouthguard Biosensor for Continuous Salivary Monitoring of Metabolites. *Analyst* **2014**, *139*, 1632−1636.

(14) Kassal, P.; Kim, J.; Kumar, R.; de Araujo, W. R.; Steinberg, I. M.; Steinberg, M. D.; Wang, J. Smart Bandage with Wireless Connectivity for Uric Acid Biosensing as an Indicator of Wound Status. *Electrochem. Commun.* **2015**, *56*, 6−10.

(15) Kim, J.; Imani, S.; de Araujo, W. R.; Warchall, J.; Valdés-Ramírez, G.; Paixão, T. R. L. C.; Mercier, P. P.; Wang, J. Wearable Salivary Uric Acid Mouthguard Biosensor with Integrated Wireless Electronics. *Biosens. Bioelectron.* **2015**, *74*, 1061−1068.

(16) Kim, J.; Jeerapan, I.; Imani, S.; Cho, T. N.; Bandodkar, A.; Cinti, S.; Mercier, P. P.; Wang, J. Noninvasive Alcohol Monitoring Using a Wearable Tattoo-Based Iontophoretic-Biosensing System. *ACS Sens.* **2016**, *1*, 1011−1019.

(17) Parrilla, M.; Cánovas, R.; Jeerapan, I.; Andrade, F. J.; Wang, J. A Textile-Based Stretchable Multi-Ion Potentiometric Sensor. *Adv. Healthcare Mater.* **2016**, *5*, 996−1001.

(18) Nyein, H. Y. Y.; Gao, W.; Shahpar, Z.; Emaminejad, S.; Challa, S.; Chen, K.; Fahad, H. M.; Tai, L.-C.; Ota, H.; Davis, R. W.; Javey, A. A Wearable Electrochemical Platform for Noninvasive Simultaneous Monitoring of Ca^{2+} and pH. *ACS Nano* **2016**, *10*, 7216−7224.

(19) Guinovart, T.; Valdés-Ramírez, G.; Windmiller, J. R.; Andrade, F. J.; Wang, J. Bandage-Based Wearable Potentiometric Sensor for Monitoring Wound pH. *Electroanalysis* **2014**, *26*, 1345−1353.

(20) Kim, J.; Cho, T. N.; Valdés-Ramírez, G.; Wang, J. A Wearable Fingernail Chemical Sensing Platform: pH Sensing at Your Fingertips. *Talanta* **2016**, *150*, 622−628.
(21) Bandodkar, A. J.; Molinnus, D.; Mirza, O.; Guinovart, T.; Windmiller, J. R.; Valdés-Ramírez, G.; Andrade, F. J.; Schöning, M. J.; Wang, J. Epidermal Tattoo Potentiometric Sodium Sensors with Wireless Signal Transduction for Continuous Non-Invasive Sweat Monitoring. *Biosens. Bioelectron.* **2014**, *54*, 603−609.
(22) Guinovart, T.; Bandodkar, A. J.; Windmiller, J. R.; Andrade, F. J.; Wang, J. A Potentiometric Tattoo Sensor for Monitoring Ammonium in Sweat. *Analyst* **2013**, *138*, 7031−7038.
(23) Kim, J.; de Araujo, W. R.; Samek, I. A.; Bandodkar, A. J.; Jia, W.; Brunetti, B.; Paixão, T. R. L. C.; Wang, J. Wearable Temporary Tattoo Sensor for Real-Time Trace Metal Monitoring in Human Sweat. *Electrochem. Commun.* **2015**, *51*, 41−45.
(24) Gao, W.; Nyein, H. Y. Y.; Shahpar, Z.; Fahad, H. M.; Chen, K.; Emaminejad, S.; Gao, Y.; Tai, L.-C.; Ota, H.; Wu, E.; Bullock, J.; Zeng, Y.; Lien, D.-H.; Javey, A. Wearable Microsensor Array for Multiplexed Heavy Metal Monitoring of Body Fluids. *ACS Sens.* **2016**, *1*, 866−874.
(25) Bariya, M.; Nyein, H. Y. Y.; Javey, A. Wearable Sweat Sensors. *Nat. Electron.* **2018**, *1*, 160−171.
(26) Choi, J.; Ghaffari, R.; Baker, L. B.; Rogers, J. A. Skin-Interfaced Systems for Sweat Collection and Analytics. *Sci. Adv.* **2018**, *4*, No. eaar3921.
(27) Kim, D.-H.; Lu, N.; Ma, R.; Kim, Y.-S.; Kim, R.-H.; Wang, S.; Wu, J.; Won, S. M.; Tao, H.; Islam, A.; Yu, K. J.; Kim, T.-i.; Chowdhury, R.; Ying, M.; Xu, L.; Li, M.; Chung, H.-J.; Keum, H.; McCormick, M.; Liu, P.; Zhang, Y.-W.; Omenetto, F. G.; Huang, Y.; Coleman, T.; Rogers, J. A. Epidermal Electronics. *Science* **2011**, *333*, 838−843.
(28) Moon, G. D.; Lim, G.-H.; Song, J. H.; Shin, M.; Yu, T.; Lim, B.; Jeong, U. Highly Stretchable Patterned Gold Electrodes Made of Au Nanosheets. *Adv. Mater.* **2013**, *25*, 2707−2712.
(29) Jang, K.-I.; Chung, H. U.; Xu, S.; Lee, C. H.; Luan, H. W.; Jeong, J.; Cheng, H. Y.; Kim, G. T.; Han, S. Y.; Lee, J. W.; Kim, J.; Cho, M.; Miao, F. X.; Yang, Y. Y.; Jung, H. N.; Flavin, M.; Liu, H.; Kong, G. W.; Yu, K. J.; Rhee, S. I.; Chung, J.; Kim, B.; Kwak, J. W.; Yun, M. H.; Kim, J. Y.; Song, Y. M.; Paik, U.; Zhang, Y. H.; Huang, Y.; Rogers, J. A. Soft Network Composite Materials with Deterministic and Bio-Inspired Designs. *Nat. Commun.* **2015**, *6*, 6566.
(30) Bandodkar, A. J.; Nuñez-Flores, R.; Jia, W.; Wang, J. All-Printed Stretchable Electrochemical Devices. *Adv. Mater.* **2015**, *27*, 3060−3065.
(31) Rogers, J. A.; Someya, T.; Huang, Y. Materials and Mechanics for Stretchable Electronics. *Science* **2010**, *327*, 1603−1607.
(32) Toghill, K. E.; Compton, R. G. Electrochemical Non-Enzymatic Glucose Sensors: A Perspective and an Evaluation. *Int. J. Electrochem. Sci.* **2010**, *5*, 1246−1301.
(33) Park, S.; Boo, H.; Chung, T. D. Electrochemical Non-Enzymatic Glucose Sensors. *Anal. Chim. Acta* **2006**, *556*, 46−57.
(34) Lee, H.-B.; Bae, C.-W.; Duy, L. T.; Sohn, I.-Y.; Kim, D.-I.; Song, Y.-J.; Kim, Y.-J.; Lee, N.-E. Mogul-Patterned Elastomeric Substrate for Stretchable Electronics. *Adv. Mater.* **2016**, *28*, 3069−3077.
(35) Nery, E. W.; Kundys, M.; Jelen, P. S.; Jonsson-Niedziolka, M. Electrochemical Glucose Sensing: Is There Still Room for Improvement? *Anal. Chem.* **2016**, *88*, 11271−11282.
(36) Park, S.; Chung, T. D.; Kim, H. C. Nonenzymatic Glucose Detection Using Mesoporous Platinum. *Anal. Chem.* **2003**, *75*, 3046−3049.
(37) Hanif, A.; Trung, T. Q.; Siddiqui, S.; Toi, P. T.; Lee, N.-E. Stretchable, Transparent, Tough, Ultrathin, and Self-limiting Skin-like Substrate for Stretchable Electronics. *ACS Appl. Mater. Interfaces* **2018**, *10*, 27297−27307.
(38) Sinatra, N. R.; Ranzani, T.; Vlassak, J. J.; Parker, K. K.; Wood, R. J. Nanofiber-Reinforced Soft Fluidic Micro-Actuators. *J. Micromech. Microeng.* **2018**, *28*, 084002.
(39) Choi, J.; Xue, Y.; Xia, W.; Ray, T. R.; Reeder, J. T.; Bandodkar, A. J.; Kang, D.; Xu, S.; Huang, Y.; Rogers, J. A. Soft, Skin-Mounted Microfluidic Systems for Measuring Secretory Fluidic Pressures Generated at The Surface of The Skin by Eccrine Sweat Glands. *Lab Chip* **2017**, *17*, 2572−2580.
(40) Berthier, E.; Beebe, D. J. Flow Rate Analysis of A Surface Tension Driven Passive Micropump. *Lab Chip* **2007**, *7*, 1475−1478.
(41) Walker, G. M.; Beebe, D. J. A Passive Pumping Method for Microfluidic Devices. *Lab Chip* **2002**, *2*, 131−134.
(42) Zimmermann, M.; Schmid, H.; Hunziker, P.; Delamarche, E. Capillary Pumps for Autonomous Capillary Systems. *Lab Chip* **2007**, *7*, 119−125.
(43) Wittstock, A.; Biener, J.; Bäumer, M. Nanoporous Gold: A New Material for Catalytic and Sensor Applications. *Phys. Chem. Chem. Phys.* **2010**, *12*, 12919−12930.
(44) Seker, E.; Reed, M.; Begley, M. Nanoporous Gold: Fabrication, Characterization, and Applications. *Materials* **2009**, *2*, 2188−2215.
(45) Pia, G.; Delogu, F. Mechanical Properties of Nanoporous Au: From Empirical Evidence to Phenomenological Modeling. *Metals* **2015**, *5*, 1665−1694.
(46) Hodge, A. M.; Hayes, J. R.; Caro, J. A.; Biener, J.; Hamza, A. V. Characterization and Mechanical Behavior of Nanoporous Gold. *Adv. Eng. Mater.* **2006**, *8*, 853−857.

DOI: 10.1021/acsami.9b00848
ACS Appl. Mater. Interfaces 2019, 11, 14567−14575